LIMNOLOGY AND OCEANOGRAPHY
Letters

ASLO
Open Access

Limnology and Oceanography Letters 2024

doi: 10.1002/lol2.10409

LETTER

Idiosyncratic phenology of greenhouse gas emissions in a Mediterranean reservoir

Eva Rodríguez-Velasco[1,2] *Ignacio Peralta-Maraver*[1,2] *Andrés Martínez-García*[1,2] *Miriam García-Alguacil*[1,2] *Félix Picazo*[1,2] *Rodrigo J. Gonçalves*[1,2] *Cintia L. Ramón*[2,3] *Rafael Morales-Baquero*[1] *Francisco J. Rueda*[2,3] *Isabel Reche*[1,2]*

[1]Departamento de Ecología and Instituto del Agua, Universidad de Granada, Granada, Spain; [2]Research Unit Modeling Nature (MNat), Universidad de Granada, Granada, Spain; [3]Departamento de Ingeniería Civil, Universidad de Granada, Granada, Spain

Scientific Significance Statement

Reservoirs are important sources of greenhouse gases (GHGs) impacting the global carbon cycle. Global change is increasing surface water temperatures, prolonging stratification, and enhancing eutrophication with uncertain consequences for future GHG emissions. Reducing the uncertainty of current predictive models requires incorporating the phenological variability in GHG emissions across latitude. This need is particularly pertinent in the Mediterranean zone, where extreme seasonal fluctuations characterize the hydrological and thermal regimes. In the Mediterranean reservoir studied, the GHG emissions were more variable than in reservoirs of other latitudes and mainly driven by water temperature, mean depth, and biological productivity. However, the relationship between CO_2 emissions and temperature was more complex. Our results suggest that future scenarios with higher temperatures, drought, and biological productivity will likely increase CH_4 emissions.

Abstract

Extreme hydrological and thermal regimes characterize the Mediterranean zone and can influence the phenology of greenhouse gas (GHG) emissions in reservoirs. Our study examined the seasonal changes in GHG emissions of a shallow, eutrophic, hardwater reservoir in Spain. We observed distinctive seasonal patterns for each gas. CH_4 emissions substantially increased during stratification, influenced predominantly by the increase in water temperature, net ecosystem production, and the decline in reservoir mean depth. N_2O emissions mirrored CH_4's seasonal trend, significantly correlating to water temperature, wind speed, and gross primary production. Conversely, CO_2 emissions decreased during stratification and displayed a quadratic, rather than a linear relationship with water

*Correspondence: ireche@ugr.es

Associate editor: Emily H. Stanley

Author Contribution Statement: IR, RM-B, and FJR conceived the study and obtained the funds. ER-V led the fieldwork and the measurements of greenhouse gas emissions with the help of IP-M, AM-G, MG-A, FP, RJG, CLR, RM-B, FJR, and IR. ER-V, IP-M, and CLR performed the data analysis and graphical representation of the results. ER-V and IR wrote the first draft of the manuscript, and all authors contributed significantly to the preparation of the final draft.

Data Availability Statement: Additional Supporting Information can be found in the online version of this article, including an extended version of methods and supplementary tables. The dataset associated with this paper is available from dryad (https://doi.org/10.5061/dryad.cnp5hqcbz).

Additional Supporting Information may be found in the online version of this article.

temperature—an unexpected deviation from CH_4 and N_2O emission patterns—likely associated with photosynthetic uptake of bicarbonate and formation of intracellular calcite that might be exported to sediments. This investigation highlights the imperative of integrating these idiosyncratic patterns into GHG emissions models, enhancing their predictive power.

Inland waters, including reservoirs, are important sources of greenhouse gases (GHGs) such as CO_2, CH_4, and N_2O (Tranvik et al. 2009; Bastviken et al. 2011; Raymond et al. 2013; Soued et al. 2016; León-Palmero et al. 2020*a*). The global estimations of GHG emissions from reservoirs range from 1.25 to 2.3 Pg CO_2 equivalents per year (Lauerwald et al. 2023). However, these global estimations are still substantially uncertain because of the idiosyncrasy of each gas—with specific external forcing and internal drivers—and the limited availability of temporal data across latitudes. Although there have been some recent attempts to describe the temporal variability of CO_2 emissions using eddy covariance techniques (Golub et al. 2023) and to model CH_4 temporal variability (Johnson et al. 2021; Zhuang et al. 2023), most available data were obtained under fair weather conditions and thus do not include the full range of variability of natural systems (Liu et al. 2016; Ran et al. 2021). Phenology (i.e., seasonal changes) differs from tropical (high and uniform temperature) to boreal (low temperature) latitudes. Therefore, input data in models should incorporate the specific, phenological drivers of GHG emissions across latitudes to reduce uncertainty. This need is especially pertinent in the warm temperate dry climatic zone (including Mediterranean zone), where extreme seasonal fluctuations characterize the hydrological and thermal regimes, and reservoirs are more prevalent than lakes (Lehner and Döll 2004; Lehner et al. 2011).

Previous studies of CO_2 emissions have not shown consistent phenological patterns yet. These emissions can be higher (Yang et al. 2013; Zhao et al. 2013; Podgrajsek et al. 2016) or lower (Shao et al. 2015; Pu et al. 2020; Amanatidou et al. 2023) during the summer than the fall–winter regardless of the reservoir latitude. These incongruent patterns are likely related to local drivers of CO_2 emissions. For instance, Yang et al. (2013) and Golub et al. (2023) found a positive relationship between temperature and CO_2 fluxes in subtropical and temperate reservoirs. It is well known that high water temperatures reduce gas solubility, promoting CO_2 release from surface waters. Moreover, seasonal changes in primary production can also modify the CO_2 exchange with the atmosphere. CO_2 assimilation by photosynthetic microorganisms decreases the dissolved CO_2 in the water and, likely, reduces emissions Pacheco et al. (2014). Zhao et al. (2013) and Pu et al. (2020) also found significant negative correlations between CO_2 fluxes and chlorophyll *a* (Chl *a*). However, this influence appears to be evident only in low-carbonate reservoirs (León-Palmero et al. 2020*a*). Temperature also affects the balance between primary production and microbial respiration. All these studies suggest that external forcing (climate) and internal drivers (carbonate–bicarbonate availability, biological productivity) interact to control CO_2 emissions, making scaling relationships challenging.

In the case of CH_4, the maximum emissions are consistently reported during the warm or shoulder seasons (Samiotis et al. 2018; Linkhorst et al. 2020; León-Palmero et al. 2020*a*; Johnson et al. 2021). The release of CH_4 by direct ebullition from the sediments generally shows this regular seasonal pattern that is related to higher hypolimnetic temperature and lower water level that facilitates ebullition (DelSontro et al. 2010; Linkhorst et al. 2020; León-Palmero et al. 2020*a*; Waldo et al. 2021*b*). Other studies correlate Chl *a* concentration with CH_4 emissions (Zhao et al. 2013; Harrison et al. 2017; Beaulieu et al. 2019; Deemer and Holgerson 2021). Particulate organic matter derived from phytoplankton appears to be an essential substrate for methanogenesis (West et al. 2015; Martínez-García et al. 2024). Therefore, climatic forcing, water level and Chl *a* affect CH_4 emissions under a more predictable pattern across latitudes (Johnson et al. 2021).

N_2O emissions also show a consistent temporal pattern with the highest emissions during summer, at least in subtropical reservoirs (Zhu et al. 2013; Musenze et al. 2014; Yang et al. 2023). However, this pattern can be modified by other factors such as dissolved oxygen concentrations, since high dissolved oxygen concentrations can inhibit denitrification and stimulate nitrification (Zhao et al. 2013; Yang et al. 2023). Furthermore, N_2O emissions may also be influenced by the availability of nutrients and organic matter. For instance, León-Palmero et al. (2020*a*, 2023) found that nitrogen and phosphorus inputs in the reservoirs increase N_2O concentration and emission because they can affect denitrifying bacteria activity (Zhu et al. 2013).

In general, water temperature is a common driver for all GHG emissions. However, the intensity of this factor and the concurrence of other drivers can modulate the net GHG emissions, making such emissions very idiosyncratic. Disentangling these drivers is relevant since recent studies point towards more extended stratification periods (Woolway and Merchant 2019) with widespread deoxygenation in the hypolimnion (Jane et al. 2021), more frequent heatwaves (Woolway et al. 2021), and an increase of eutrophication (Beaulieu et al. 2019).

Here, we determined the seasonal changes of CO_2, CH_4, and N_2O emissions in a Mediterranean reservoir. We hypothesize that the GHG emissions would be higher in summer than in winter due to increasing temperatures. CH_4 ebullition and N_2O emissions will be accentuated in the summertime due also to reduction of water level and development of anoxic conditions in the hypolimnion.

Materials and methods

Cubillas is a shallow, hardwater, eutrophic reservoir located in the southeast of Spain (37°16′34″N, 3°40′24″W) with a surface of 194.4 ha and a capacity of 13.53 hm^3. The reservoir has uniform bathymetry (Supporting Information Fig. S1). The annual water level fluctuated approximately 3 m, with the lowest values during fall. The main reservoir uses are irrigation and recreation.

To describe the GHGs phenology in this reservoir, we monitored the fluxes of CO_2, CH_4 (diffusive and ebullitive), and N_2O weekly from March 2021 to July 2022. We determined CO_2, CH_4, and N_2O fluxes using a Cavity Ring-Down Spectrometer PICARRO G2508 connected to a floating chamber placed on the water surface. On each sampling day, we took 4–6 measurements throughout the daytime at the same location (Supporting Information Fig. S1). We calculated fluxes as in Zhao et al. (2015) (Supporting Information). For the CH_4 fluxes, we also discriminate between diffusion and ebullition using an adaptation of the algorithm proposed by Hoffmann et al. (2017) (Supporting Information). The CO_2 equivalent emissions were calculated by multiplying the mass-based flux (in units of mg CO_2, CH_4, or N_2O m^{-2} d^{-1}) by the 100-yr global warming potential of each gas (1 for CO_2, 27 for CH_4, and 273 for N_2O; IPCC 2022).

We recorded the water temperature, oxygen concentration, and water depth using a SeaBird 19 plus profiler. We determined the strength of the thermal stratification (*see* Supporting Information Fig. S2 and the related text). To obtain the wind speed data, we used a Davis® Wind Speed and Direction Smart Sensor and a Campbell Scientific WindSonic2. We determined the nitrate concentrations using ion chromatography. We calculated gross primary production (GPP), respiration (Res), and net ecosystem production (NEP) using the diel oxygen method proposed by Staehr et al. (2010) and data recorded using a PME miniDOT probe (10 min resolution) and a TriOS Dissolved Oxygen Sensor (1 min resolution) located at 1 m depth (Supporting Information).

We explored the potential drivers for each gas using linear mixed-effects models (LMM) including sampling date as a random factor. We selected several variables as potential fixed predictors, including water temperature, wind speed, water level, GPP, NEP, and nitrate concentration. The two-level factor "period" (stratification vs. mixing) was excluded in all models. This factor was strongly correlated with temperature (Supporting Information).

Results and discussion

The study reservoir always acted as a source of CO_2, CH_4, and N_2O (i.e., all fluxes were positive). The CO_2 emissions ranged from 12.5 to 567.02 mg C m^{-2} d^{-1} (Fig. 1a). We did not find significant differences in the CO_2 fluxes between the stratification and mixing periods ($t = 0.6$, df = 62, p-value = 0.55) (Fig. 1b). These values are similar to other temperate reservoirs (Barros et al. 2011; Morales-Pineda et al. 2014; Deemer et al. 2016; León-Palmero et al. 2020*a*). The highest emissions were observed during spring and fall and immediately after the disruption of Saharan dust deposition (*see* black arrows in Fig. 1a). This reservoir experiences recurrent Saharan dust intrusions that transport phosphorus and organic matter boosting bacterial and primary productivity (Morales-Baquero et al. 2006; Reche et al. 2009; De Vicente et al. 2012). Therefore, these peaks in CO_2 emissions associated with Saharan dust deposition could be related to an enhancement of bacterial metabolism with respect to primary production. The lowest emissions were observed during the summer. This seasonal pattern has been also observed in other Mediterranean reservoirs which even found negative fluxes (i.e., CO_2 uptake) during summertime (Samiotis et al. 2018; Montes-Pérez et al. 2022) and in other subtropical (Yang et al. 2013; Pu et al. 2020) and boreal (Demarty and Tremblay 2019) reservoirs. However, this pattern is less consistent in other Northern-temperate (> 50°N) reservoirs with higher emissions during summertime (Golub et al. 2023).

The total CH_4 emissions ranged from 0.23 to 1204.82 mg C m^{-2} d^{-1} (Fig. 1c, green dots), being significantly higher ($t = 7.9$, df = 61, p-value < 0.001) during the stratification than during the mixing period (Fig. 1d). These values are higher than those found in most tropical and Northern-temperate reservoirs (Barros et al. 2011; Deemer et al. 2016) and represent an upper limit in the emissions reported for the Mediterranean reservoirs (Samiotis et al. 2018; León-Palmero et al. 2020*a*; Montes-Pérez et al. 2022). The diffusive fluxes ranged from 0.23 to 472.09 mg C m^{-2} d^{-1} (Fig. 1c, yellow dots), whereas the ebullitive fluxes ranged from 0 to 1200.89 mg C m^{-2} d^{-1}. The ebullition contribution to the total CH_4 emissions was lower than 20% during the mixing period, whereas it was usually higher than 70% during the stratification period accounting for up to 99.8% of the total fluxes for some of the summer sampling dates. These results are similar to those obtained in shallow reservoirs in Northern-temperate, Mediterranean, and tropical latitudes (Keller and Stallard 1994; DelSontro et al. 2010, 2011; Miller et al. 2017; Montes-Pérez et al. 2022) but higher than the emissions measured in deep reservoirs (DelSontro et al. 2011).

The N_2O fluxes ranged from 0 to 670.92 μg N m^{-2} d^{-1} (Fig. 1e). We observed higher emissions during August, but without significant differences between the stratification and the mixing period ($t = 0.7$, df = 64, p-value = 0.49) (Fig. 1f). These values are similar to those found in boreal, Northern-temperate, Mediterranean, and subtropical reservoirs (Liu et al. 2011; Musenze et al. 2014; Soued et al. 2016; Descloux et al. 2017; Liang et al. 2019; León-Palmero et al. 2020*a*).

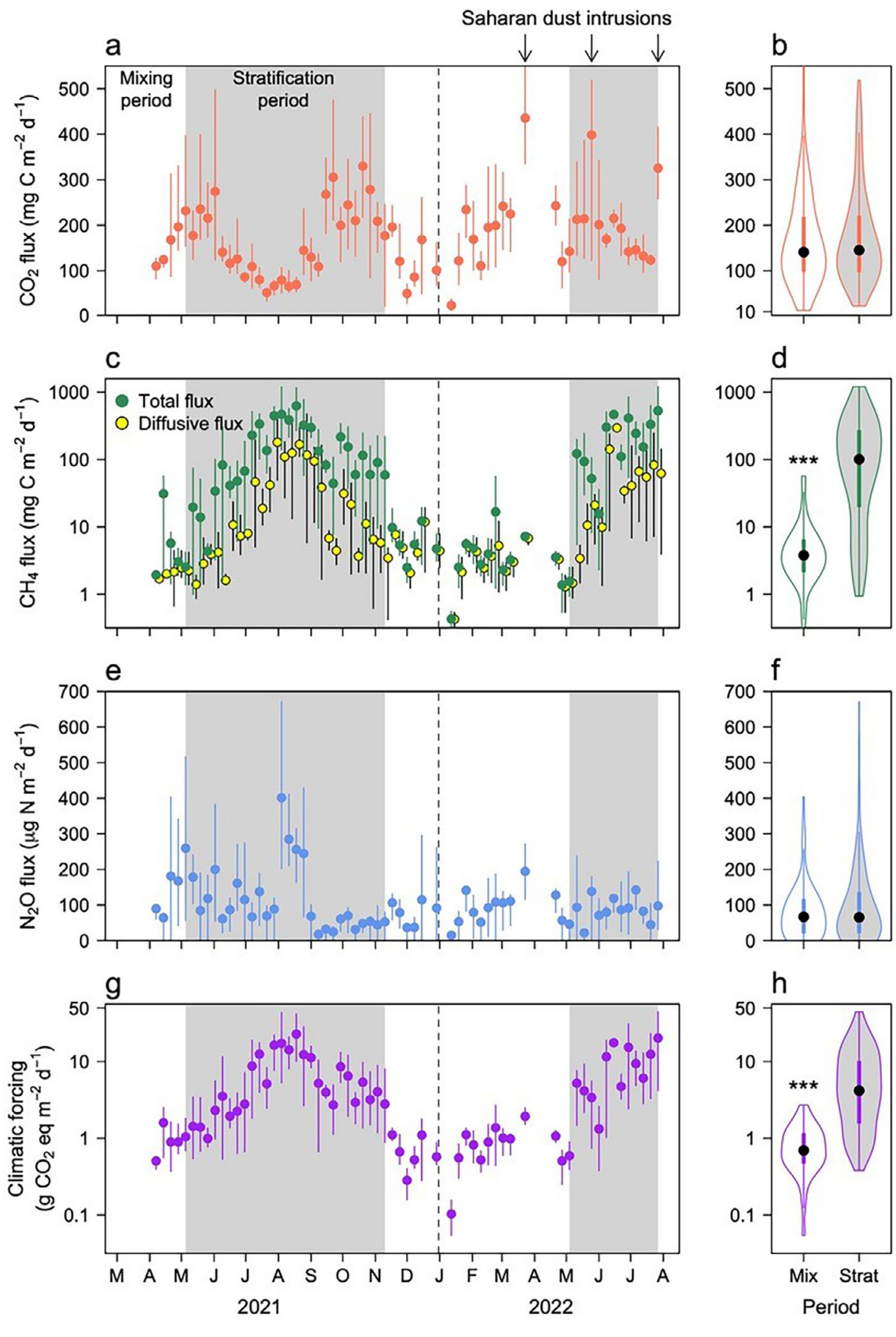

Fig. 1. Seasonal changes in the CO_2 emissions (**a**) and the violin plots for the distribution of values during the mixing and stratification periods (**b**), seasonal changes in the CH_4 total (green dots) and diffusive (yellow dots) emissions (**c**) and the violin plots for the distribution of values during the mixing and stratification periods of total CH_4 emissions (**d**), seasonal changes in N_2O emissions (**e**) and the violin plots for the distribution of values during the mixing and stratification periods (**f**), and the seasonal changes in the climatic forcing due to CO_2, CH_4 and N_2O emissions expressed in CO_2 equivalents in the Cubillas reservoir (**g**) and the violin plots for the distribution of values during the mixing and stratification periods (**h**). In the time series, dots are the mean daily values from four to six measurements and the whiskers are the minimum and maximum values. In the violin plots, black dots are the median, bars are the quartile 25–75%, and ***$p < 0.001$. Note the logarithmic scale for the CH_4 emissions and the climatic forcing to improve visualization and the units of climatic forcing in g CO_2 equivalent. Dotted vertical lines represent the change from year 2021 to 2022. [Correction added on June 4, 2024, after initial online publication: In Figure 1, the part figure 1d has been replaced in this version.]

The climatic forcing due to emissions of the three GHGs was maximum during summer, reaching more than 10,000 mg CO_2 eq $m^{-2}\,d^{-1}$ (Fig. 1g) with significantly more climatic forcing during stratified conditions than when the reservoir was mixed ($t = 7.8$, $df = 61$, p-value < 0.001) (Fig. 1h). Overall, we found the maximum climatic forcing during the summer due to the CH_4 and N_2O emissions.

In the case of CO_2 emissions, the main fixed drivers included surface water temperature and wind speed (details of the LMM in Supporting Information Table S1). The surface water temperature ranged from 8.92°C to 28.52°C (Fig. 2a). The wind speed ranged from 0 to 6.38 m s^{-1} (Fig. 2b). Unexpectedly, the relationship between CO_2 emissions and water temperature was quadratic (Fig. 2c). The CO_2 emissions increased with the temperature up to approximately 20°C and then decreased at higher temperatures. This result differs from the previous ones reported in the literature, where the relationship between CO_2 emissions and temperature appears linear and positive (Yang et al. 2013; Zhao et al. 2013; Golub et al. 2023). This phenomenon could be related to the fact that in hardwater systems, as the study reservoir, dissolved inorganic carbon available for photosynthesis is mainly in the form of HCO_3^-. Some species of microalgae and cyanobacteria have developed a mechanism that increases the bicarbonate inside the cells at the carboxysome, where some enzymes (e.g., carbonic anhydrase) convert this HCO_3^- into CO_2 to photosynthesis (Moroney and Ynalvez 2007). Therefore, photosynthesis coupled to calcite formation removes two bicarbonates: one HCO_3^- for calcite formation ($CaCO_3 + H^+$) and the other one for photosynthesis that converts HCO_3^- into CO_2 and then in organic matter. Intracellular calcite formation during photosynthesis induces a substantial decrease in bicarbonate and does not release CO_2 into the water column. In hardwater reservoirs, seasons or locations with high photosynthesis have been linked to calcite formation further suggesting that the coupling of the two processes may be an overlooked C sink with a substantial reduction in alkalinity (Deemer et al. 2020; Escoffier et al. 2023; Perolo et al. 2023). High temperatures promote cyanobacteria blooms (Paerl and Paul 2012) and, consequently, during summertime, this process could be accentuated, and CO_2 emissions reduced. López et al. (2011) showed that carbonate precipitation in summertime affects the metabolism–CO_2 emission relationship, and Waldo et al. (2021*a*) found that the best predictors of CO_2 emissions were surface pH and bicarbonate concentrations. The CO_2 emissions also showed a positive linear correlation with the wind speed (Fig. 2d). The higher wind speeds will increase CO_2 emissions since wind intensity promotes gas transfer from the water surface to the atmosphere. This observation is consistent with previous studies on the circadian scale (Liu et al. 2016).

The main fixed predictors of the diffusive CH_4 emissions were water temperature (Fig. 3a,d), water level (Fig. 3b,e), and NEP (Fig. 3c,f) (Supporting Information Table S1). Water level ranged from 636.16 to 639.46 m above sea level (i.e., from 3.01 to 6.26 m depth), and NEP ranged from 0.06 to 1.04 mg C L^{-1} d^{-1}. In the case of the ebullitive fluxes, the main predictors were only water temperature (Fig. 3a,g) and water level (Fig. 3b,h). These robust correlations between water temperature and diffusive and ebullitive CH_4 emissions agree with previous studies (Yang et al. 2013; Yvon-Durocher et al. 2014;

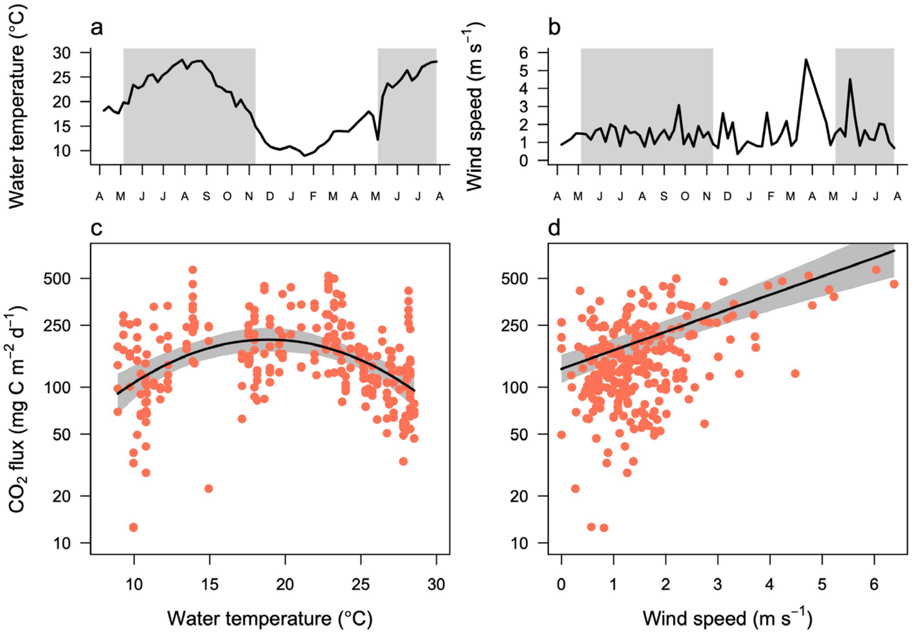

Fig. 2. LMMs for the main drivers of the CO_2 fluxes. Time series of water temperature (**a**) and wind speed (**b**). CO_2 emission as a function of water temperature (**c**) and wind speed (**d**). The red dots are the observations ($n = 268$), the black lines are the fit lines, and the gray areas are the 95% confidence intervals. Conditional $R^2 = 0.72$; marginal $R^2 = 0.36$.

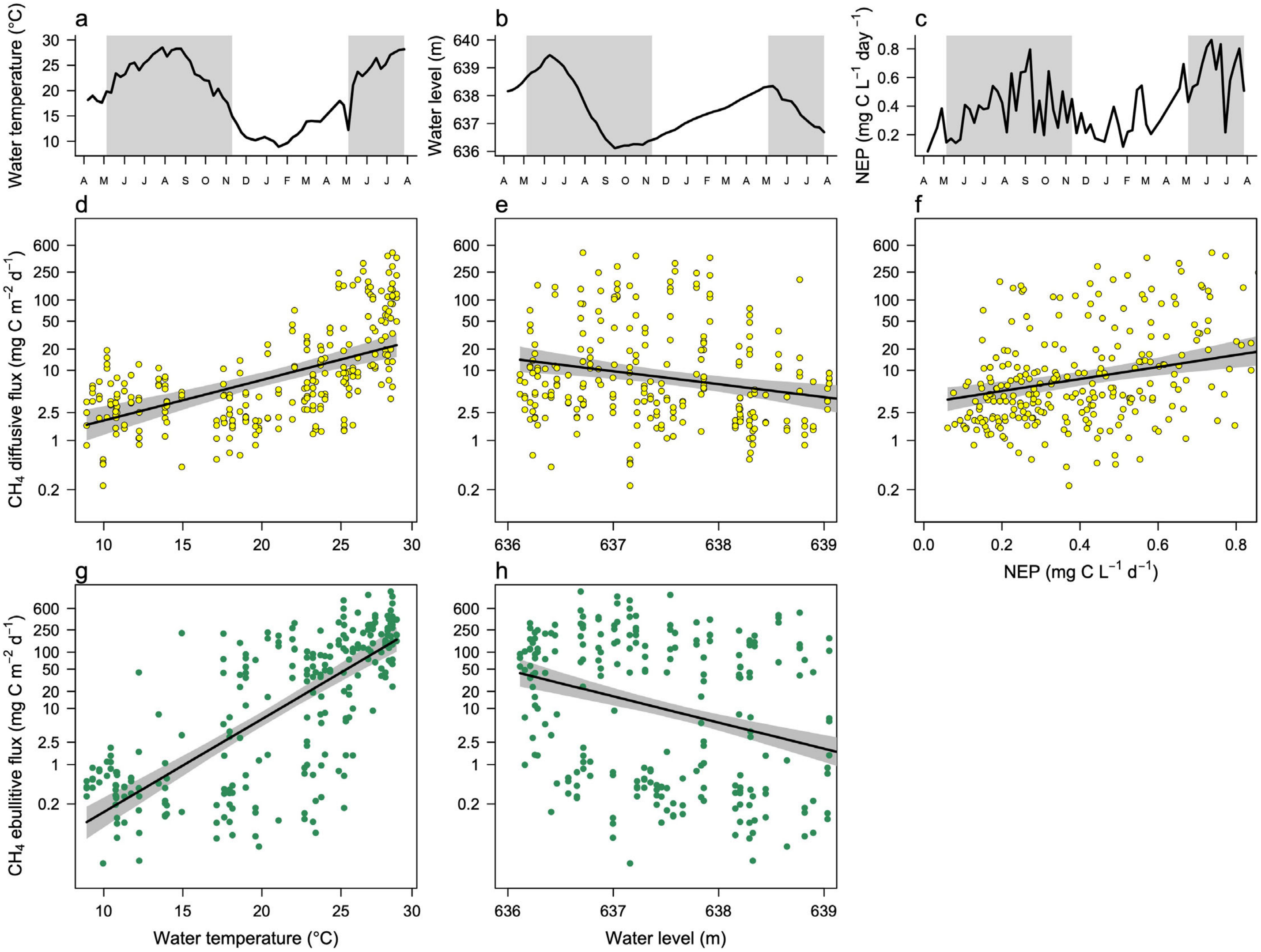

Fig. 3. LMMs for the main drivers of the CH_4 diffusive (conditional $R^2 = 0.74$; marginal $R^2 = 0.48$) and ebullitive fluxes (conditional $R^2 = 0.72$; marginal $R^2 = 0.63$). Time series of water temperature (**a**), water level (**b**), and NEP (**c**). CH_4 diffusive emission as function of water temperature (**d**), water level (**e**), and NEP (**f**). The yellow dots are the observations ($n = 268$), the black lines are the fit lines, and the gray areas are the 95% confidence intervals. CH_4 ebullitive flux as a function of water temperature (**g**) and water level (**h**). The green dots are the observations ($n = 250$), the black lines are the fit lines, and the gray areas are the 95% confidence intervals. Water level means meters above sea level.

Mosher et al. 2015; Linkhorst et al. 2020). High temperatures can intensify CH_4 emissions due to changes in solubility and an increase in sediment methanogenesis (Duc et al. 2010; Yvon-Durocher et al. 2014). In the study reservoir, this relationship is even steeper for the ebullitive flux (slope = 0.17) than for the diffusive flux (slope = 0.06) (Supporting Information Table S1; Fig. 3d,g). The effect of temperature on CH_4 emissions is maybe more noticeable in shallow systems, as the heat is transferred more efficiently throughout the water column to the sediments (Natchimuthu et al. 2016). The water level (i.e., hydrostatic pressure) was negatively correlated with both fluxes (Fig. 3e,h). This predictor, like the temperature, was more influential in the ebullition fluxes with a higher slope (−0.46) than in the diffusion fluxes with a lower slope (−0.18) (Supporting Information Table S1). Previous studies have also reported similar results (DelSontro et al. 2011; Xiao et al. 2013; Harrison et al. 2017; Linkhorst et al. 2020; León-Palmero et al. 2020*a*). Harrison et al. (2017) and Beaulieu et al. (2018) showed that water level decline triggers the release of CH_4-rich bubbles from the sediments. Finally, the diffusive flux was also positively correlated with NEP (Fig. 3f). There are at least two non-exclusive underlying mechanisms to explain this relationship. First, there is evidence of a direct link between CH_4 production and photosynthesis by picoeukaryotes and cyanobacteria in surface waters (e.g., Klintzsch et al. 2019; Bižić et al. 2020; León-Palmero et al. 2020*b*), and previous works have reported maximum fluxes associated with spring algae blooms (Waldo et al. 2021*b*). Second, methanogenesis in sediments appears to be boosted by phytoplanktonic organic matter exported to sediments (West et al. 2015, 2016). Indeed, we have observed a lagged response between phytoplankton-derived particulate organic matter and methane emissions in the study reservoir (Martínez-García et al. 2024). Similarly, Bertolet et al. (2020) found a relationship between the CH_4 storage in the hypolimnion and the GPP. This result could explain why we did not find a synchronous relationship between NEP and the CH_4 ebullitive flux. This pattern with maximum CH_4 emissions during summer was also observed in previous studies of temperate latitudes (Jacinthe et al. 2012; Beaulieu et al. 2014; McClure et al. 2020), and it differs from that observed in boreal lakes with peaks shortly after ice-off (Denfeld et al. 2018), in other temperate lakes with peaks during the fall mixing (Encinas Fernández et al. 2013) or in reservoirs that experience flood control drawdowns (Harrison et al. 2017).

The main fixed drivers of N_2O emissions were water temperature (Fig. 4a,d), wind speed (Fig. 4b,e), and GPP (Fig. 4c,f) (Supporting Information Table S1). The GPP values ranged from 0.22 to 3.29 mg C L^{-1} d^{-1} (Fig. 4c). Surprisingly, we did not find a significant relationship between the N_2O emissions and nitrate and these emissions decreased with increases of GPP. Previous studies have also shown positive relationships between N_2O emissions and temperature (Zhu et al. 2013; Musenze et al. 2014; Xiao et al. 2019; Yang et al. 2023) associated with increased microbial activity. An increment in wind speed also stimulates the transference of N_2O to the atmosphere. León-Palmero et al. (2020*a*) also reported a relevant influence of wind speed on N_2O emissions. In previous studies, however, positive correlations between Chl *a* concentration (that could be considered as a surrogate of primary production) and the emission of N_2O have been reported (Xiao et al. 2019).

All the results above highlight the importance of temperature in the Mediterranean zone as a driver of the three GHGs, although the quadratic function obtained for CO_2 emissions needs further exploration to unravel its ultimate causes. Furthermore, autochthonous production only correlated synchronously with diffusive CH_4 emissions, but surprisingly not with CO_2 emissions.

Finally, we compared our results (black and white triangles in Fig. 5) with previous studies that reported GHG seasonal dynamics in reservoirs and lakes across latitudes (Supporting Information Tables S2–S4). In the case of CO_2 fluxes (Fig. 5a), the variability range was broader—including negative fluxes—in tropical/subtropical (0° to 30°), temperate low latitudes (light orange bands 30° to 45°) that include the Mediterranean zone, and temperate high latitudes (45° to 60°) than in the boreal (> 60°) latitude that presented a lower amplitude. In the case of CH_4 fluxes (Fig. 5b), all values were always positive (i.e., CH_4 sources). The most wide-ranging variability was also found in the systems from the 30°–45° latitudes (light orange bands), and the lowest ones in the boreal systems (Fig. 5b). The same observation was also reported by Johnson et al. (2021) using a

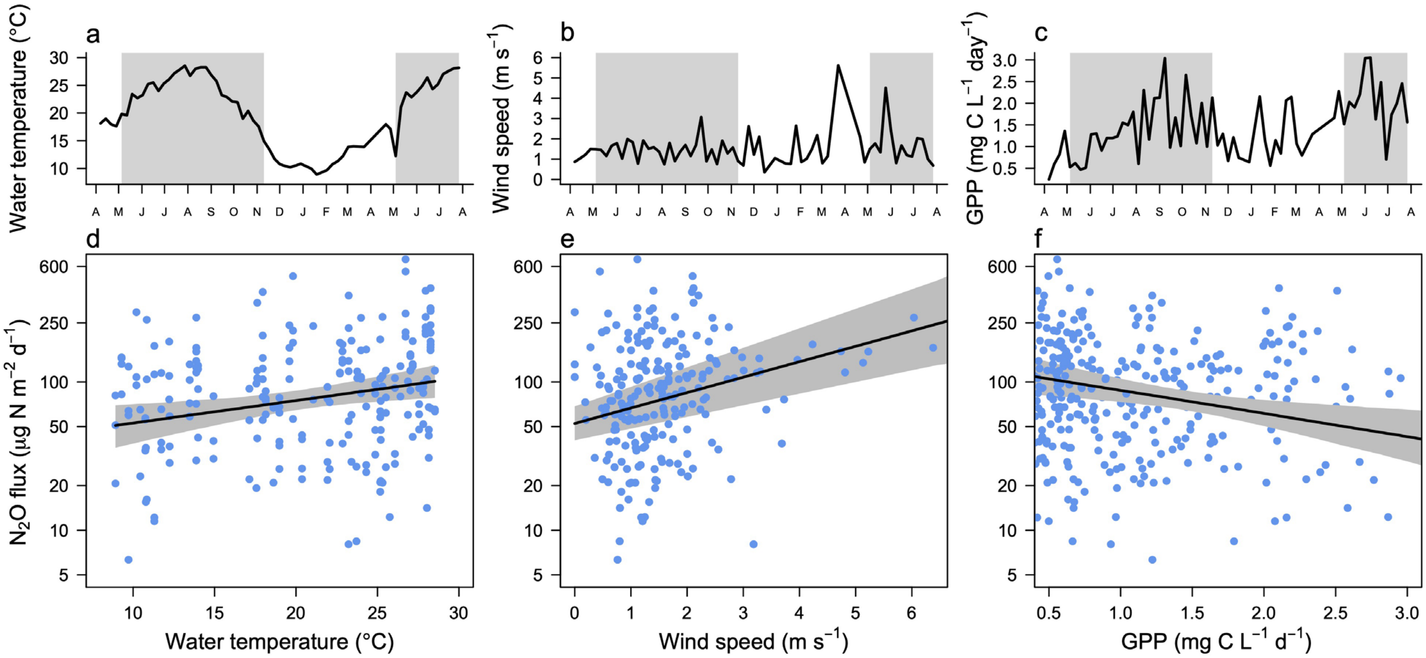

Fig. 4. LMMs for the main drivers of the N_2O fluxes. Time series of water temperature (**a**), wind speed (**b**), and GPP (**c**). N_2O emission as function of water temperature (**d**), wind speed (**e**), and GPP (**f**). The blue dots are the observations ($n = 218$), the black lines are the fit lines, and the gray areas are the 95% confidence intervals. Conditional $R^2 = 0.46$; marginal $R^2 = 0.13$.

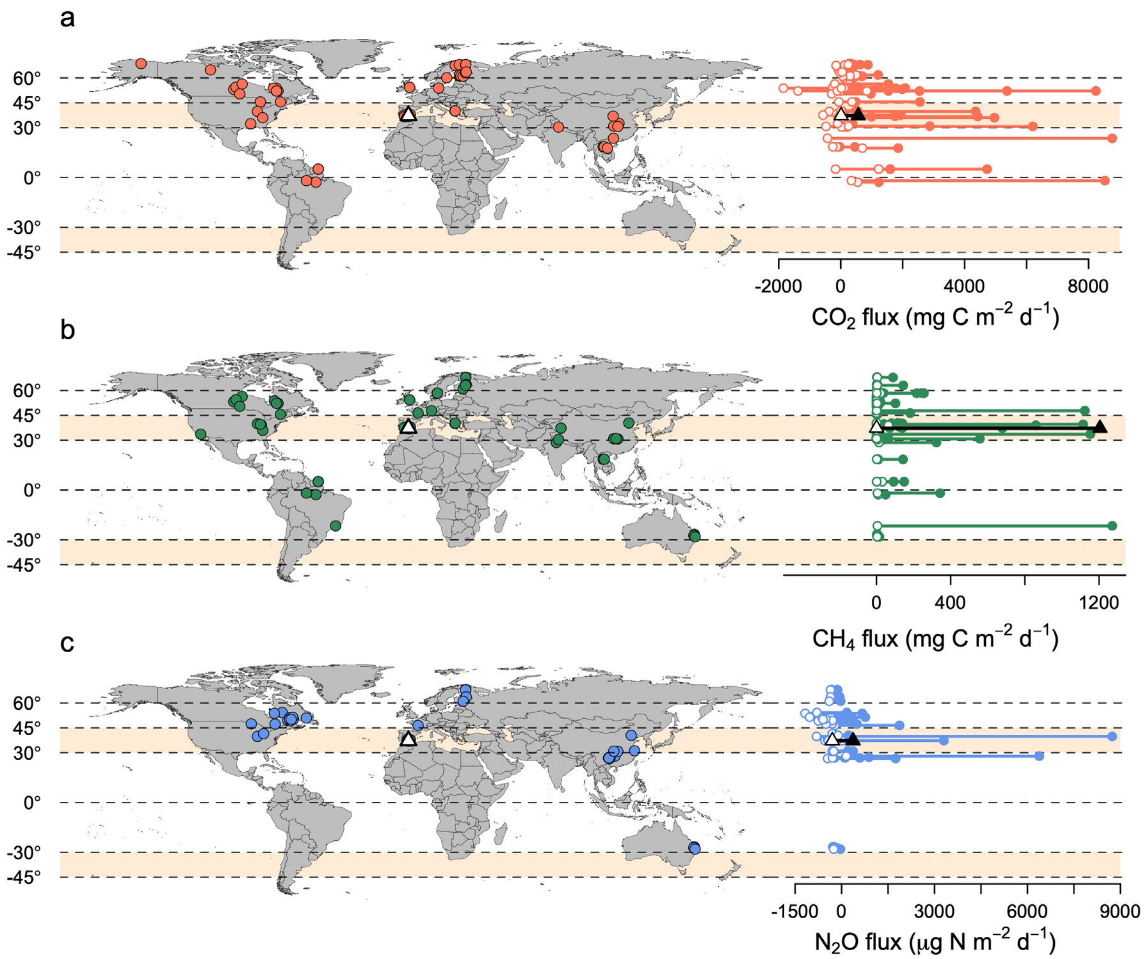

Fig. 5. Locations of the reservoirs and lakes with temporal variability of CO_2 (orange dots), CH_4 (green dots), and N_2O (blue dots) fluxes found in the literature (Supporting Information Tables S2–S4) and our study reservoir (white triangle). The magnitude of seasonal variability in the fluxes is represented by the line, the white dots represent the minimum values and the colored dots the maximum values, including the negative values for CO_2 fluxes (**a**) CH_4 fluxes (**b**), and N_2O fluxes (**c**). The variability of the study reservoir is represented by a line with white (minimum values) and black (maximum values) triangles. The temperate low latitude from 30° to 45° (including the Mediterranean zone) is represented with a light orange shadow.

different approach. For N_2O fluxes (Fig. 5c), the most extensive variability—including negative fluxes—was also observed in the systems located at 30° to 45° latitudes, and the smallest again in the boreal latitudes. Despite the lack of data for some regions, this comparison emphasizes the relevance of including seasonal variability, particularly from temperate low latitudes from 30° to 45°, in the upscaling models and exploring local drivers that can be easily obtained using remote sensing approaches such as primary productivity and inundation surface. In addition, new models should consider other sources of variability not included here, such as the differences in fluxes between day and night (Liu et al. 2016; Golub et al. 2023) and the high spatial variability in some reservoir fluxes (Colas et al. 2020; Linkhorst et al. 2020; Liu et al. 2021). This model improvement could provide more accurate projections under future scenarios of increasing temperatures and more extended stratification periods (Woolway and Merchant 2019) resulting in anoxic hypolimnia (Jane et al. 2021), which can enhance methanogenesis and denitrification, as well as more severe eutrophication (Beaulieu et al. 2019).

References

Amanatidou, E., G. Samiotis, E. Trikoilidou, L. Tsikritzis, and N. Taousanidis. 2023. Centennial assessment of greenhouse gases emissions of young and old hydroelectric reservoir in mediterranean Mainland. J Environ Inf. **41**: 27. doi:10.3808/jei.202300485

Barros, N., J. J. Cole, L. J. Tranvik, Y. T. Prairie, D. Bastviken, V. L. M. Huszar, P. A. Del Giorgio, and F. Roland. 2011. Carbon emission from hydroelectric reservoirs linked to reservoir age and latitude. Nat. Geosci. **4**: 593–596. doi:10.1038/ngeo1211

Bastviken, D., L. J. Tranvik, J. A. Downing, P. M. Crill, and A. Enrich-Prast. 2011. Freshwater methane emissions offset the continental carbon sink. Science **331**: 50. doi:10.1126/science.1196808

Beaulieu, J. J., R. L. Smolenski, C. T. Nietch, A. Townsend-Small, and M. S. Elovitz. 2014. High methane emissions from a midlatitude reservoir draining an agricultural watershed. Environ. Sci. Tech. **48**: 11100–11108. doi:10.1021/es501871g

Beaulieu, J. J., and others. 2018. Effects of an experimental water-level drawdown on methane emissions from a eutrophic reservoir. Ecosystems **21**: 657–674. doi:10.1007/s10021-017-0176-2

Beaulieu, J. J., T. DelSontro, and J. A. Downing. 2019. Eutrophication will increase methane emissions from lakes and impoundments during the 21st century. Nat. Commun. **10**: 1375. doi:10.1038/s41467-019-09100-5

Bertolet, B. L., C. R. Olson, D. K. Szydlowski, C. T. Solomon, and S. E. Jones. 2020. Methane and primary productivity in lakes: Divergence of temporal and spatial relationships. J. Geophys. Res. Biogeosci. **125**: e2020JG005864. doi:10.1029/2020JG005864

Bižić, M., and others. 2020. Aquatic and terrestrial cyanobacteria produce methane. Sci. Adv. **6**: eaax5343. doi:10.1126/sciadv.aax5343

Colas, F., V. Chanudet, M. Daufresne, L. Buchet, R. Vigouroux, A. Bonnet, F. Jacob, and J. Baudoin. 2020. Spatial and temporal variability of diffusive CO_2 and CH_4 fluxes from the Amazonian Reservoir Petit-Saut (French Guiana) reveals the importance of allochthonous inputs for long-term C emissions. Global Biogeochem. Cycl. **34**. doi:10.1029/2020gb006602

De Vicente, I., E. Ortega-Retuerta, R. Morales-Baquero, and I. Reche. 2012. Contribution of dust inputs to dissolved organic carbon and water transparency in Mediterranean reservoirs. Biogeosciences **9**: 5049–5060. doi:10.5194/bg-9-5049-2012

Deemer, B. R., and others. 2016. Greenhouse gas emissions from reservoir water surfaces: A new global synthesis. Bioscience **66**: 949–964. doi:10.1093/biosci/biw117

Deemer, B. R., E. G. Stets, and C. B. Yackulic. 2020. Calcite precipitation in Lake Powell reduces alkalinity and total salt loading to the Lower Colorado River Basin. Limnol. Oceanogr. **65**: 1439–1455. doi:10.1002/lno.11399

Deemer, B. R., and M. A. Holgerson. 2021. Drivers of methane flux differ between lakes and reservoirs, complicating global upscaling efforts. J. Geophys. Res. Biogeosci. **126**: e2019JG005600. doi:10.1029/2019JG005600

DelSontro, T., D. F. McGinnis, S. Sobek, I. Ostrovsky, and B. Wehrli. 2010. Extreme methane emissions from a swiss hydropower reservoir: Contribution from bubbling sediments. Environ. Sci. Technol. **44**: 2419–2425. doi:10.1021/es9031369

DelSontro, T., M. J. Kunz, T. Kempter, A. Wüest, B. Wehrli, and D. B. Senn. 2011. Spatial heterogeneity of methane ebullition in a large tropical reservoir. Environ. Sci. Tech. **45**: 9866–9873. doi:10.1021/es2005545

Demarty, M., and A. Tremblay. 2019. Long term follow-up of pCO_2, pCH_4 and emissions from Eastmain 1 boreal reservoir, and the Rupert diversion bays, Canada. Ecohydrol. Hydrobiol. **19**: 529–540. doi:10.1016/j.ecohyd.2017.09.001

Denfeld, B. A., H. M. Baulch, P. A. del Giorgio, S. E. Hampton, and J. Karlsson. 2018. A synthesis of carbon dioxide and methane dynamics during the ice-covered period of northern lakes. Limnol. Oceanogr. Lett. **3**: 117–131. doi:10.1002/lol2.10079

Descloux, S., V. Chanudet, D. Serça, and F. Guérin. 2017. Methane and nitrous oxide annual emissions from an old eutrophic temperate reservoir. Sci. Total Environ. **598**: 959–972. doi:10.1016/j.scitotenv.2017.04.066

Duc, N. T., P. Crill, and D. Bastviken. 2010. Implications of temperature and sediment characteristics on methane formation and oxidation in lake sediments. Biogeochemistry **100**: 185–196. doi:10.1007/s10533-010-9415-8

Encinas Fernández, J., F. Peeters, and H. Hofmann. 2013. Importance of the autumn overturn and anoxic conditions in the hypolimnion for the annual methane emissions from a temperate lake. Environ. Sci. Technol. **48**: 7297–7304. doi:10.1021/es4056164

Escoffier, N., P. Perolo, G. Many, N. T. Pasche, and M. E. Perga. 2023. Fine-scale dynamics of calcite precipitation in a large hardwater lake. Sci. Total Environ. **864**: 160699. doi:10.1016/j.scitotenv.2022.160699

Golub, M., and others. 2023. Diel, seasonal, and inter-annual variation in carbon dioxide effluxes from lakes and reservoirs. Environ. Res. Lett. **18**: 034046. doi:10.1088/1748-9326/acb834

Harrison, J. A., B. R. Deemer, and M. T. Birchfield. 2017. Reservoir water-level drawdowns accelerate and amplify methane emission. Environ. Sci. Tech. **51**: 1267–1277. doi:10.1021/acs.est.6b03185

Hoffmann, M., M. Schulz-Hanke, J. G. Alba, N. Jurisch, U. Hagemann, T. Sachs, M. Sommer, and J. Augustin. 2017. A simple calculation algorithm to separate high-resolution CH_4 flux measurements into ebullition- and diffusion-derived components. Atmos. Meas. Tech. **10**: 109–118. doi:10.5194/amt-10-109-2017

Intergovernmental Panel on Climate Change (IPCC), ed. 2022. Annex II: Definitions, units and conventions. *In* P. R. Shukla and others [eds.], *IPCC, 2022: Climate change 2022: Mitigation of climate change. Contribution of Working Group III to the Sixth Assessment Report of the Intergovernmental Panel on Climate Change* (pp.1821-1840). Cambridge University Press. doi:10.1017/9781009157926.021

Jacinthe, P., Filippelli, G. M., Tedesco, L. P., and Raftis, R. 2012. Carbon storage and greenhouse gases emission from a fluvial reservoir in an agricultural landscape. Catena. **94**: 53–63. doi:10.1016/j.catena.2011.03.012

Jane, S. F., and others. 2021. Widespread deoxygenation of temperate lakes. Nature **594**: 66–70. doi:10.1038/s41586-021-03550-y

Johnson, M. S., E. Matthews, D. Bastviken, B. Deemer, J. Du, and V. Genovese. 2021. Spatiotemporal methane emission from global reservoirs. J. Geophys. Res. Biogeosci. **126**. doi:10.1029/2021jg006305

Keller, M., and R. F. Stallard. 1994. Methane emission by bubbling from Gatun Lake, Panama. J. Geophys. Res. **99**: 8307–8319. doi:10.1029/92jd02170

Klintzsch, T., G. Langer, G. Nehrke, A. Wieland, K. Lenhart, and F. Keppler. 2019. Methane production by three widespread marine phytoplankton species: Release rates, precursor compounds, and potential relevance for the environment. Biogeosciences **16**: 4129–4144. doi:10.5194/bg-16-4129-2019

Lauerwald, R., and others. 2023. Inland water greenhouse gas budgets for RECCAP2: 1. State-of-the-art of global scale assessments. Global Biogeochem. Cycles **37**: e2022GB007657. doi:10.1029/2022GB007657

Lehner, B., and P. Döll. 2004. Development and validation of a global database of lakes, reservoirs and wetlands. J. Hydrol. **296**: 1–22. doi:10.1016/j.jhydrol.2004.03.028

Lehner, B., and others. 2011. High-resolution mapping of the world's reservoirs and dams for sustainable river-flow management. Front. Ecol. Environ. **9**: 494–502. doi:10.1890/100125

León-Palmero, E., R. Morales-Baquero, and I. Reche. 2020*a*. Greenhouse gas fluxes from reservoirs determined by watershed lithology, morphometry, and anthropogenic pressure. Environ. Res. Lett. **15**: 044012. doi:10.1088/1748-9326/ab7467

León-Palmero, E., A. Contreras-Ruiz, A. Sierra, R. Morales-Baquero, and I. Reche. 2020*b*. Dissolved CH_4 coupled to photosynthetic picoeukaryotes in oxic waters and to cumulative chlorophyll a in anoxic waters of reservoirs. Biogeosciences **17**: 3223–3245. doi:10.5194/bg-17-3223-2020

León-Palmero, E., R. Morales-Baquero, and I. Reche. 2023. P inputs determine denitrifier abundance explaining dissolved nitrous oxide in reservoirs. Limnol. Oceanogr. **68**: 1734–1749. doi:10.1002/lno.12381

Liang, X., T. Xing, J. Li, B. Wang, F. Wang, C. He, L. Hou, and S. Li. 2019. Control of the hydraulic load on nitrous oxide emissions from cascade reservoirs. Environ. Sci. Technol. **53**: 11745–11754. doi:10.1021/acs.est.9b03438

Linkhorst, A., C. Hiller, T. DelSontro, G. M. Azevedo, N. Barros, R. Mendonça, and S. Sobek. 2020. Comparing methane ebullition variability across space and time in a Brazilian reservoir. Limnol. Oceanogr. **65**: 1623–1634. doi:10.1002/lno.11410

Liu, H., Q. Zhang, G. G. Katul, J. J. Cole, F. S. Chapin, and S. Macintyre. 2016. Large CO_2 effluxes at night and during synoptic weather events significantly contribute to CO_2 emissions from a reservoir. Environ. Res. Lett. **11**: 064001. doi:10.1088/1748-9326/11/6/064001

Liu, J., S. Xiao, C. Wang, Z. Yang, D. Liu, X. Guo, L. Liu, and A. Lorke. 2021. Spatial and temporal variability of dissolved methane concentrations and diffusive emissions in the Three Gorges Reservoir. Water Res. **207**: 117788. doi:10.1016/j.watres.2021.117788

Liu, Y., R. Zhu, D. Ma, H. Xu, Y. Luo, T. Huang, and L. Sun. 2011. Temporal and spatial variations of nitrous oxide fluxes from the littoral zones of three alga-rich lakes in coastal Antarctica. Atmos. Environ. **45**: 1464–1475. doi:10.1016/j.atmosenv.2010.12.017

López, P., R. Marcé, and J. Armengol. 2011. Net heterotrophy and CO_2 evasion from a productive calcareous reservoir: Adding complexity to the metabolism-CO_2 evasion issue. J. Geophys. Res. **116**: G02021. doi:10.1029/2010JG001614

Martínez-García, A., and others. 2024. Particulate organic carbon sedimentation triggers lagged methane emissions in a eutrophic reservoir. Limnol. Oceanogr. Lett. doi:10.1002/lol2.10379

McClure, R. P., M. E. Lofton, S. Chen, K. M. Krueger, J. C. Little, and C. C. Carey. 2020. The magnitude and drivers of methane ebullition and diffusion vary on a longitudinal gradient in a small freshwater reservoir. J. Geophys. Res. Biogeosci. **125**: e2019JG005205. doi:10.1029/2019JG005205

Miller, B. L., E. V. Arntzen, A. E. Goldman, and M. C. Richmond. 2017. Methane ebullition in temperate hydropower reservoirs and implications for US policy on greenhouse gas emissions. Environ. Manag. **60**: 615–629. doi:10.1007/s00267-017-0909-1

Montes-Pérez, J. J., B. Obrador, T. Conejo-Orosa, V. Rodríguez, R. Marcé, C. Escot, I. Reyes, J. Rodriguez, and E. Moreno-Ostos. 2022. Spatio-temporal variability of carbon dioxide and methane emissions from a Mediterranean reservoir. Limnetica **41**: 43–60. doi:10.23818/limn.41.04

Morales-Baquero, R., E. Pulido-Villena, and I. Reche. 2006. Atmospheric inputs of phosphorus and nitrogen to the southwest Mediterranean region: Biogeochemical responses of high mountain lakes. Limnol. Oceanogr. **51**: 830–837. doi:10.4319/lo.2006.51.2.0830

Morales-Pineda, M., A. Cózar, I. Laiz, B. Úbeda, and J. A. Gálvez. 2014. Daily, biweekly, and seasonal temporal scales of pCO_2 variability in two stratified Mediterranean reservoirs. J. Geophys. Res. Biogeo. **119**: 509–520. doi:10.1002/2013jg002317

Moroney, J. V., and R. A. Ynalvez. 2007. Proposed carbon dioxide concentrating mechanism in *Chlamydomonas reinhardtii*. Eukaryot. Cell **6**: 1251–1259. doi:10.1128/ec.00064-07

Mosher, J. J., A. M. Fortner, J. R. Phillips, M. S. Bevelhimer, A. D. Stewart, and M. J. Troia. 2015. Spatial and temporal correlates of greenhouse gas diffusion from a hydropower reservoir in the southern United States. Water **7**: 5910–5927. doi:10.3390/w7115910

Musenze, R. S., A. Grinham, U. Werner, D. Gale, K. Sturm, J. Udy, and Z. Yuan. 2014. Assessing the spatial and temporal variability of diffusive methane and nitrous oxide emissions from subtropical freshwater reservoirs. Environ. Sci. Tech. **48**: 14499–14507. doi:10.1021/es505324h

Natchimuthu, S., I. Sundgren, M. Gålfalk, L. Klemedtsson, P. Crill, Å. Danielsson, and D. Bastviken. 2016. Spatio-temporal variability of lake CH_4 fluxes and its influence on annual whole lake emission estimates. Limnol. Oceanogr. **61**: S13–S26. doi:10.1002/lno.10222

Pacheco, F. S., Roland, F., & Downing, J. A. 2014. Eutrophication reverses whole-lake carbon budgets. Inland waters. **4**: 41–48. doi:10.5268/IW-4.1.614

Paerl, H. W., and V. J. Paul. 2012. Climate change: Links to global expansion of harmful cyanobacteria. Water Res. **46**: 1349–1363. doi:10.1016/j.watres.2011.08.002

Perolo, P., N. Escoffier, H. E. Chmiel, G. Many, D. Bouffard, and M. E. Perga. 2023. Alkalinity contributes at least a third of annual gross primary production in a deep stratified hardwater lake. Limnol. Oceanogr. Lett. **8**: 359–367. doi:10.1002/lol2.10311

Podgrajsek, E., E. Sahlée, D. Bastviken, S. Natchimuthu, N. Kljun, H. E. Chmiel, L. Klemedtsson, and A. Rutgersson. 2016. Methane fluxes from a small boreal lake measured with the eddy covariance method. Limnol. Oceanogr. **61**: S41–S50. doi:10.1002/lno.10245

Pu, J., J. Li, T. Zhang, J. B. Martin, and D. Yuan. 2020. Varying thermal structure controls the dynamics of CO_2 emissions from a subtropical reservoir, south China. Water Res. **178**: 115831. doi:10.1016/j.watres.2020.115831

Ran, L., D. Butman, T. J. Battin, X. Yang, M. Tian, C. Duvert, J. Hartmann, N. Geeraert, and S. Liu. 2021. Substantial decrease in CO_2 emissions from Chinese inland waters due to global change. Nat. Commun. **12**: 1730. doi:10.1038/s41467-021-21926-6

Raymond, P. A., and others. 2013. Global carbon dioxide emissions from inland waters. Nature **503**: 355–359. doi:10.1038/nature12760

Reche, I., E. Ortega-Retuerta, O. Romera, E. Pulido-Villena, R. Morales-Baquero, and E. O. Casamayor. 2009. Effect of Saharan dust inputs on bacterial activity and community composition in Mediterranean lakes and reservoirs. Limnol. Oceanogr. **54**: 869–879. doi:10.4319/lo.2009.54.3.0869

Samiotis, G., G. Pekridis, N. Kaklidis, E. Trikoilidou, N. Taousanidis, and E. Amanatidou. 2018. Greenhouse gas emissions from two hydroelectric reservoirs in Mediterranean region. Environ. Monit. Assess. **190**: 363. doi:10.1007/s10661-018-6721-4

Shao, C., J. Chen, C. A. Stepien, H. Chu, Z. Ouyang, T. B. Bridgeman, … and R. John. 2015. Diurnal to annual changes in latent, sensible heat, and CO_2 fluxes over a Laurentian Great Lake: A case study in Western Lake Erie. J. Geophys. Res. Biogeosci. **120**: 1587–1604. doi:10.1002/2015JG003025

Soued, C., P. A. del Giorgio, and R. Maranger. 2016. Nitrous oxide sinks and emissions in boreal aquatic networks in Québec. Nat. Geosci. **9**: 116–120. doi:10.1038/ngeo2611

Staehr, P. A., D. L. Bade, M. C. Van De Bogert, G. R. Koch, C. Williamson, P. Hanson, J. J. Cole, and T. Kratz. 2010. Lake metabolism and the diel oxygen technique: State of the science. Limnol. Oceanogr. Methods **8**: 628–644. doi:10.4319/lom.2010.8.0628

Tranvik, L. J., and others. 2009. Lakes and reservoirs as regulators of carbon cycling and climate. Limnol. Oceanogr. **54**: 2298–2314. doi:10.4319/lo.2009.54.6_part_2.2298

Waldo, S., B. R. Deemer, L. S. Bair, and J. J. Beaulieu. 2021*a*. Greenhouse gas emissions from an arid-zone reservoir and their environmental policy significance: Results from existing global models and an exploratory dataset. Environ. Sci. Policy **120**: 53–62. doi:10.1016/j.envsci.2021.02.006

Waldo, S., J. J. Beaulieu, W. Barnett, D. A. Balz, M. J. Vanni, T. Williamson, and J. T. Walker. 2021*b*. Temporal trends in methane emissions from a small eutrophic reservoir: The key role of a spring burst. Biogeosciences **18**: 5291–5311. doi:10.5194/bg-18-5291-2021

West, W. E., S. M. McCarthy, and S. E. Jones. 2015. Phytoplankton lipid content influences freshwater lake methanogenesis. Freshw. Biol. **60**: 2261–2269. doi:10.1111/fwb.12652

West, W. E., K. P. Creamer, and S. E. Jones. 2016. Productivity and depth regulate lake contributions to atmospheric methane. Limnol. Oceanogr. **61**: S51–S61. doi:10.1002/lno.10247

Woolway, R. I., and C. J. Merchant. 2019. Worldwide alteration of lake mixing regimes in response to climate change. Nat. Geosci. **12**: 271–276. doi:10.1038/s41561-019-0322-x

Woolway, R. I., E. Jennings, T. Shatwell, M. Golub, D. C. Pierson, and S. C. Maberly. 2021. Lake heatwaves under climate change. Nature **589**: 402–407. doi:10.1038/s41586-020-03119-1

Xiao, Q., X. Xu, M. Zhang, H. Duan, Z. Hu, W. Wang, W. Xiao, and X. Lee. 2019. Coregulation of nitrous oxide emissions by nitrogen and temperature in China's third largest freshwater lake (Lake Taihu). Limnol. Oceanogr. **64**: 1070–1086. doi:10.1002/lno.11098

Xiao, S., D. Liu, Y. Wang, Z. Yang, and W. Chen. 2013. Temporal variation of methane flux from Xiangxi Bay of the Three Gorges Reservoir. Sci. Rep. **3**: 2500. doi:10.1038/srep02500

Yang, F., C. Sun, H. Wang, X. Hu, S. Wang, M. Zhang, L. Zhang, and J. Zhong. 2023. Significant spatiotemporal variability of nitrous oxide emissions from a temperate reservoir experiencing intensive aquaculture disturbance. Agric. Ecosyst. Environ. **348**: 108427. doi:10.1016/j.agee.2023.108427

Yang, L., F. Lu, X. Wang, X. Duan, L. Tong, Z. Ouyang, and H. Li. 2013. Spatial and seasonal variability of CO_2 flux at the air-water interface of the Three Gorges Reservoir. J. Environ. Sci. **25**: 2229–2238. doi:10.1016/s1001-0742(12)60291-5

Yvon-Durocher, G., A. P. Allen, D. Bastviken, R. Conrad, C. Gudasz, A. St-Pierre, N. Thanh-Duc, and P. A. Del Giorgio.

2014. Methane fluxes show consistent temperature dependence across microbial to ecosystem scales. Nature **507**: 488–491. doi:10.1038/nature13164

Zhao, Y., B. F. Wu, and Y. Zeng. 2013. Spatial and temporal patterns of greenhouse gas emissions from Three Gorges Reservoir of China. Biogeosciences **10**: 1219–1230. doi:10.5194/bg-10-1219-2013

Zhao, Y., and others. 2015. A comparison of methods for the measurement of CO_2 and CH_4 emissions from surface water reservoirs: Results from an international workshop held at Three Gorges Dam, June 2012. Limnol. Oceanogr. Methods **13**: 15–29. doi:10.1002/lom3.10003

Zhu, D., and others. 2013. Nitrous oxide emissions from the surface of the Three Gorges Reservoir. Ecol. Eng. **60**: 150–154. doi:10.1016/j.ecoleng.2013.07.049

Zhuang, Q., M. Guo, J. M. Melack, X. Lan, Z. Tan, Y. Oh, and L. R. Leung. 2023. Current and future global lake methane emissions: A process-based modeling analysis. J. Geophys. Res. Biogeosci. **128**: e2022JG007137. doi:10.1029/2022JG007137

Acknowledgments

The authors thank the reviewers and the associate editor for their notable contributions to improving this manuscript. The grant PID2022.1378650B.100 funded by MICIU/AEI/10.13039/501100011033/ and by ERDF, EU. ER-V and AM-G were supported by Ph.D. fellowships FPU 19/02161 and FPU20/05804 respectively from the Spanish Ministry of Science, Innovation, and Universities. IP-M and FP are PAIDI postdoctoral fellows funded by Junta de Andalucía. RJG was funded by a María Zambrano grant from the Spanish Ministry of Universities and Next Generation European Union funds. [Correction added on June 4, 2024, after initial online publication: In Acknowledgement section, the sentence “This research was funded by the projects CRONOS (RTI2018-098849-B-I00), and ANTICIPA (PID2022- 137865OB-I00) of Spanish Ministry of Science, Innovation, and Universities to IR and FJR.” has been replaced with "The grant PID2022.1378650B.100 funded by MICIU/AEI/10.13039/501100011033/ and by ERDF, EU." in this version.]

Submitted 29 May 2023
Revised 30 April 2024
Accepted 03 May 2024